






# Novel “late potential map” algorithm: Abnormal potentials and scar channels detection for ventricular tachycardia ablation

Nuno Cortez-Dias MD, PhD<sup>1,2</sup>  | Gustavo Lima da Silva MD<sup>1,2</sup>  |  
 Afonso Nunes-Ferreira MD<sup>1,2</sup>  | Elad Nakar MSc<sup>3</sup> | Raquel Francisco MSc<sup>4</sup> |  
 Mariana Pereira MSc<sup>5</sup> | Luís Carpinteiro MD<sup>1,2</sup> | Fausto J. Pinto MD, PhD<sup>1,2</sup>  |  
 João de Sousa MD<sup>1,2</sup> 

<sup>1</sup>Cardiology Department, Lisbon Academic Medical Centre, Santa Maria University Hospital (CHULN), Lisbon, Portugal

<sup>2</sup>Cardiac Rhythm Abnormalities Unit, Cardiovascular Centre of the University of Lisbon, Lisbon School of Medicine of the Universidade de Lisboa, Lisbon, Portugal

<sup>3</sup>Research and Development Department, Biosense Webster, Johnson & Johnson, Yokneam, Israel

<sup>4</sup>EMEA Clinical Development, Biosense Webster, Johnson & Johnson, Diegem, Belgium

<sup>5</sup>ClinicalSupport, Biosense Webster, Johnson & Johnson, Porto Salvo, Portugal

## Correspondence

Nuno Cortez-Dias, MD, PhD, Serviço de Cardiologia, Departamento de Coração e Vasos (CHULN), Hospital de Santa Maria, Av Prof. Egas Moniz, 1649-028 Lisbon, Portugal. Email: cortezdias@yahoo.com

**Disclosure** Drs. Nuno Cortez-Dias and João de Sousa received travel and consulting fees from Biosense Webster, Boston Scientific, and Abbott Medical. Elad Nakar is an engineer used by Biosense Webster. Raquel Francisco and Mariana Pereira are Biosense Webster employees serving as clinical specialists. Other authors: No disclosures.

## Abstract

**Background:** Automated systems for substrate mapping in the context of ventricular tachycardia (VT) ablation may annotate far-field rather than near-field signals, rendering the resulting maps hard to interpret. Additionally, quantitative assessment of local conduction velocity (LCV) remains an unmet need in clinical practice. We evaluate whether a new late potential map (LPM) algorithm can provide an automatic and reliable annotation and localized bipolar voltage measurement of ventricular electrograms (EGMs) and if LCV analysis allows recognizing intrascar conduction corridors acting as VT isthmuses.

**Methods:** In 16 patients referred for scar-related VT ablation, 8 VT activation maps and 29 high-resolution substrate maps from different activation wavefronts were obtained. In offline analysis, the LPM algorithm was compared to manually annotated substrate maps. Locations of the VT isthmuses were compared with the corresponding substrate maps in regard to LCV.

**Results:** The LPM algorithm had an overall/local abnormal ventricular activity (LAVA) annotation accuracy of 94.5%/81.1%, which compares to 83.7%/23.9% for the previous wavefront algorithm. The resultant maps presented a spatial concordance of 88.1% in delineating regions displaying LAVA. LAVA median localized bipolar voltage was 0.22 mV, but voltage amplitude assessment had modest accuracy in distinguishing LAVA from other abnormal EGMs (area under the curve: 0.676;  $p < .001$ ). LCV analysis in high-density substrate maps identified a median of two intrascar conduction corridors per patient (interquartile range: 2–3), including the one acting as VT isthmus in all cases.

**Conclusion:** The new LPM algorithm and LCV analysis may enhance substrate characterization in scar-related VT.

## KEYWORDS

ablation, conduction velocity, mapping, ventricular tachycardia

## 1 | INTRODUCTION

Catheter ablation of ventricular tachycardia (VT) in the setting of structural heart disease is commonly oriented by substrate-based treatment strategies. Automated systems for substrate mapping allow for rapid acquisition of high-resolution substrate maps.<sup>1,2</sup> However, these may annotate far-field rather than near-field signals in areas of low voltage, rendering the resulting maps hard to interpret.<sup>3</sup>

A new late potential map (LPM) software has been developed for the Carto mapping system (Biosense Webster Inc.), containing a local abnormal ventricular activity (LAVA) annotation algorithm, which aims to provide a reliable annotation of near-field signals, especially in areas of low voltage with complex electrograms (EGMs), and a more realistic bipolar voltage assessment by excluding the far-field component from the peak-to-peak voltage quantification. Additionally, it includes an algorithm for automatic regional vector analysis, allowing to determine the directionality of the electrical wavefront and display a quantitative assessment of local conduction velocity (LCV). These components aim to facilitate the recognition of the intrascar conduction corridors and to allow a less operator-dependent identification of the steep conduction slowing sites.

We aim to evaluate whether the new LPM algorithm can provide a more comprehensive and reliable annotation of ventricular EGMs, particularly in low voltage areas, making the substrate map acquisition more reproducible and less dependent on the operator skills. Specifically, we intend to evaluate the accuracy of the LPM algorithm for proper annotation of the ventricular signals in general, and in annotating LAVAs in particular, and to characterize LAVA signals in terms of the localized bipolar voltage. Finally, we present preliminary data on the use of LCV analysis to recognize intrascar conduction corridors, including the ones acting as VT isthmuses.

## 2 | METHODS

### 2.1 | Study design and population

Between 2018 and June 2020, patients referred for scar-related VT ablation at the Arrhythmia Unit of the Santa Maria University Hospital (Lisbon, Portugal) were considered eligible for this study. Inclusion criteria were the availability of a high-resolution left ventricle (LV) substrate map collected with the Pentaray<sup>®</sup> mapping catheter and Carto<sup>®</sup>3 (version 6 or 7; Biosense Webster Inc.) before any deployment of radiofrequency energy, and at least one of the following: (1) detailed activation map during VT providing appropriate delineation of the critical isthmus, additionally proved by entrainment maneuvers and, if the VT was stable and tolerated, by termination with the targeted radiofrequency application; availability of high-resolution substrate maps collected during different wavefront sources (sinus rhythm [SR], right ventricle [RV] pacing, or LV pacing).

The Institutional Ethics Committee on human research at our institution approved the collection and review of these data. The

description of the electrophysiology procedure and workflows used for substrate map collection and VT activation mapping is presented as Supporting Information.

### 2.2 | Offline analyses

#### 2.2.1 | LAVA annotation algorithm

Maps were analyzed retrospectively using a noncommercial version of the Carto<sup>®</sup>3 Version 8. Five copies of each substrate map were created, one generating the "gold-standard" manually annotated map, one to run the wavefront algorithm (used as a comparator), and the others to test the new LPM software.

The LPM software includes a LAVA annotation algorithm (LAA), which analyses all components of the unipolar signal within the window of interest (WOI) and proceeds with a sequential analysis to better discriminate the near-field signal (Figure 1). On the basis of unipolar  $dV/dT$  analysis, all the candidate components to be recognized as potential signals of interest are identified, and priority for annotation is given to the latest one if its voltage is higher than the noise level and its timing is consistent in  $\geq 2$  consecutive heartbeats. The operator programs the late boundary threshold, which sets the local activation time (LAT) value from which any candidate component becomes a priority for annotation. In this study, the late boundary threshold was set in the middle of the QRS complex in all cases. The operator has the option to adjust the unipolar  $dV/dT$  parameters used for candidate EGM components selection, impacting algorithm accuracy, with three different set modes available: standard, specific, and sensitive.

Additionally, the LAA provides a localized bipolar voltage assessment, which aims to restrict the bipolar voltage measurement to near-field signals. For that, the algorithm analyses the complete signal to determine whether it is a complex EGM (with multiple candidate components). In such cases, the WOI for localized bipolar voltage assessment surrounds the near-field LAT annotation and its left curtain is dynamically adjusted to selectively exclude any high-voltage far-field components.

**Gold-standard substrate map:** A copy of the substrate map automatically annotated by the LAA (sensitive mode) was used for manual analysis. All EGMs were reviewed by two operators (Nuno Cortez-Dias and Gustavo Lima da Silva) and a third reviewer (João de Sousa) was asked to give his interpretation in cases of discrepancies. Electronic calipers at a similar gain of 0.20 mV/cm and speed of 200 mm/s were used during EGM analysis. The LAT annotation of multicomponent EGMs was defined using the method described by Anter et al.,<sup>4</sup> which aims to better differentiate near-field from far-field signals. Basically, local potentials are expected to conduct within the tissue, thus exhibiting a spatiotemporal pattern of propagation, whereas remote potentials are generated by the sum of the surrounding EGMs and are not expected to exhibit a spatiotemporal pattern of propagation. In cases of doubt, the local EGM components were compared during different wavefront sources (SR, RV pacing, or

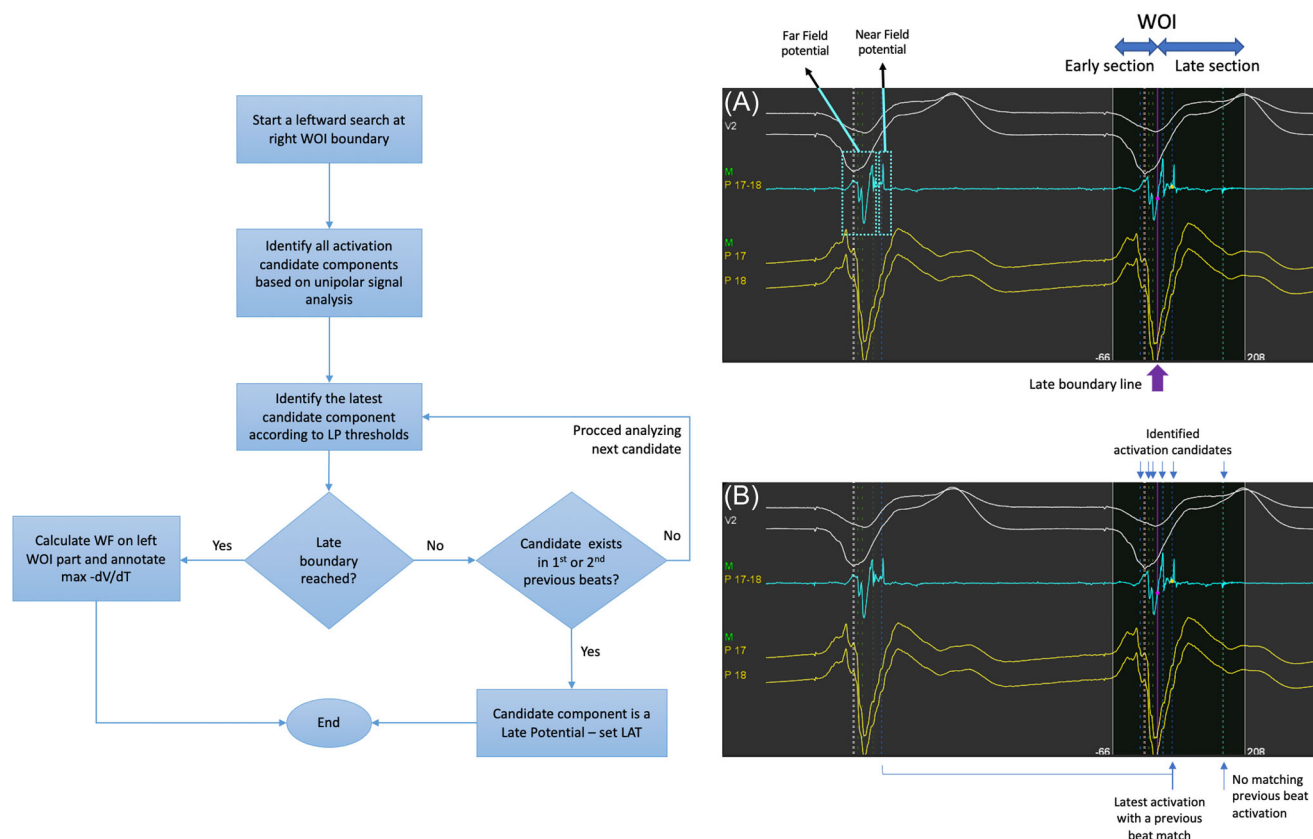


**FIGURE 1** Late potentials map (LPM) algorithm. The operator configures a temporal value (late boundary), represented by the purple late boundary line in (A) that splits the WOI into two parts. This is essential for the LPM algorithm to accurately search for late potentials. The late boundary can be adjusted during mapping and retrospectively for any selected points in the map. The algorithm starts by performing a leftward scanning of the right part of WOI to identify all relevant activation candidate components, through unipolar signal analysis. Potential candidates are signal deflections that pass a set of threshold parameters specially designed for LAVAs. Both proximal and distal electrode signals are used in finding such deflections. (B) Exemplificative signal, with all its activation candidate components. The algorithm proceeds by analyzing the latest activation candidate, to check if corresponds to a real EGM component. The first previous beat and the second previous beat are used, searching for that specific activation. If an activation exists in one of the two previous beats at a temporal position within a range of 10 ms, the candidate activity is validated as an EGM component and is annotated as a late potential. If not, the search continues to the next activation candidate. (B) The latest activation candidate (likely noise) was rejected since a similar activation is absent in the previous beats. The process continues until a candidate is found which is evident in previous beats, or the late boundary is reached. When no repetitive candidates are identified in the late section of WOI, the early section is considered to apply the standard Wavefront (WF) activation algorithm, where the strongest negative  $dV/dt$  is determined as the local activation time. EGM, electrogram; LAVA, local abnormal ventricular activity; WOI, window of interest

LV pacing) to better distinguish near-field from far-field signals. The automatic annotation was accepted if the algorithm correctly annotated the near-field component. If the automatic algorithm failed in recognizing the near-field signal, the annotation was considered inappropriate and corrected.

EGMs were classified by the operators according to the following basic descriptors (Figure S1):

1. Normal EGMs: Signals with bipolar voltage amplitude  $\geq 1.50$  mV,  $\leq 3$  intrinsic deflections, and duration  $\leq 70$  ms.
2. Isolated low-voltage EGMs: Signals with bipolar voltage amplitude  $< 1.50$  mV,  $\leq 3$  intrinsic deflections, duration  $\leq 70$  ms, without any sharp high-frequency components and occurring during the QRS complex.

3. Definite LAVA: Composite signal with at least a high-frequency potential clearly distinct from the far-field signal, occurring any time during or after the QRS complex. This category included signals usually described as isolated late potentials, split EGMs, and fractionated low-amplitude signals.
4. Intra-far-field LAVA: Composite signal with at least a high-frequency potential occurring during the far-field component.
5. Inert scar: EGM with localized bipolar voltage amplitude  $< 0.02$  mV.
6. Artifact.

In addition to the previously mentioned classification, EGMs fitting in categories 2–5 were classified as abnormal EGMs.

*Substrate maps are automatically annotated:* The remaining four copies of each substrate map were used to run the automatic EGM

annotation, without any further operator intervention, applying: 1) the standard mode; 2) the sensitive mode; 3) the “sensitive/standard” mode—sensitive in the areas with bipolar voltage <1.0 mV and standard mode in the remaining regions; and 4) the wavefront algorithm.

Annotation algorithms' accuracy was evaluated at an EGM level, by determining the proportion of signals properly annotated and misannotated, overall and by EGM category. The automatic annotation was considered accurate if the exact EGM component chosen on the “gold-standard” map was selected for annotation by the algorithm.

Additionally, the LAA performance was evaluated at the map level, by measuring the spatial concordance between the “gold-standard” map and the “sensitive/standard” mode or wavefront annotated maps regarding the regions displaying definite LAVAs. Spatial concordance was quantified by dividing the surface area covered by definite LAVAs properly annotated by the total surface area covered by definite LAVAs (properly plus misannotated) (Figure S2).

## 2.2.2 | LCV analysis

LCV algorithm determines local vectors for the regions where high-resolution characterization of the electrical wavefront is available. Each vector calculation is based on the LAT and positions of the surrounding EGM data points using a principal component analysis. The algorithm has a minimal number of point criteria within predefined radiuses and takes into consideration the temporal dispersion of the LAT values to identify conduction discontinuity. The distance between EGMs used for vector analysis is measured from the projection of the electroanatomical points on the cardiac shell. Therefore, to limit spatial inaccuracy, the cardiac shell was carefully analyzed at the area of interest, and the zones where the cardiac surface had been pushed were shaved. Vectors are displayed superimposed on the LAT map as arrows, with an origin and a direction that indicates the directionality of the local electrical wavefront. Additionally, the algorithm determines LCV at each vector and that information is graphically represented by the thickness of the arrows. The operator has the option to set the cutoff to be used in the slow conduction zones representation, ranging from 0.10 to 2 mm/ms. The algorithm depicts with thick arrows the vectors displaying LCV below the chosen threshold and with thin arrows the remaining ones, in static or dynamic displays.

Finally, the algorithm includes a compression tool, which may be set from 0 to 3, based on principal component analysis modeling of the vector information, reducing local vector dispersion, which, in turn, may help the physician to concentrate attention on the central portion possible channels. By analyzing the vectors presenting a common direction in close proximity, the compression tool searches for the dominant one, which may theoretically better locate the conducting tissue corridor.

In this study, we compared the location of the VT isthmuses with the corresponding substrate maps regarding LCV. This

analysis was restricted to the eight patients with a detailed characterization of the VT isthmus. The high-resolution VT activation maps collected during the procedures were reviewed and all the EGMs were manually corrected to the near-field signals. We evaluated whether the locations corresponding to the entrance region, common-channel, and exit region were identified as slow conduction zones during SR, RV pacing, or LV pacing, considering the following LCV cutoffs:  $\leq 0.10$ ; 0.11–0.15, 0.16–0.20, and  $> 0.20$  mm/ms. The entrance region was defined as the site where the wavefront enters an isthmus common channel. The common channel was defined as a channel bounded by two lateral lines of block or slow conduction, producing an orthodromic wavefront. The exit was defined as the site where the wavefront exits the common channel to activate the remainder ventricle. Additionally, we assessed if the locations corresponding to VT isthmuses were predicted as intrascar conduction corridors through the analysis of the local vectors superimposed on the LAT maps, testing LCV cutoffs ranging from 0.10 to 0.20 mm/ms and compression levels from 0 to 3. Intrascar conduction corridors were defined as corridors of LCV vectors with: 1)  $LCV \leq 0.20$  mm/ms; 2) localized bipolar voltage <1.50 mV; 3) length  $\geq 10$  mm; and 4) vector orientation parallel to the length of the corridor (Figure S3).

To evaluate the spatial concordance between the VT activation map and substrate maps, VT isthmus dimensions were measured in terms of length, width, and surface area with respect to the portion of the common channel with LAT values corresponding to the 25%–75% VT diastolic interval.

## 2.3 | Statistical analysis

Continuous variables are described by the mean and standard deviation for normally distributed data or median and interquartile range (IQR) for non-normally distributed data. Categorical variables are expressed as counts or percentages. Comparison of bipolar voltage by EGM category was performed using the Mann–Whitney or Kruskal–Wallis tests. Receiver operator characteristic curve analysis was used to evaluate the accuracy of localized bipolar voltage in distinguishing LAVAs amongst the remaining abnormal EGMs. Comparison of intrascar conduction corridors area as identified by LCV analysis, with the surface area harboring LAVAs in the “gold-standard” substrate map and the VT isthmus area was performed using the Wilcoxon test.  $p < .05$  was considered statistically significant. All statistical analyses were performed using SPSS version 26.0 (IBM).

## 3 | RESULTS

### 3.1 | Population and procedural characteristics

Sixteen patients fulfilled the inclusion criteria. Table 1 and Table S1 summarize their demographic characteristics. Fifteen



**TABLE 1** Baseline characteristics of the patients

| Patient characteristics <sup>a</sup>                          | N = 16            |
|---|-------------------|
| Age—year  | 66 ± 12           |
| Male sex—no. (%)  | 15 (93.8)         |
| Cause of structural heart disease                             |                   |
| Ischemic—no. (%)  | 14 (87.5)         |
| Time since last myocardial infarction—year                    | 13 ± 11           |
| Previous percutaneous revascularization—no. (%)               | 11 (78.6)         |
| Previous surgical revascularization—no. (%)                   | 2 (14.3)          |
| Nonischemic—no. (%)   | 2 (12.5)          |
| Dilated cardiomyopathy—no. (%)                                | 2 (12.5)          |
| Heart failure and comorbidities                               |                   |
| NYHA functional class   |                   |
| I/II—no. (%)  | 3 (18.8)/9 (56.3) |
| III—no. (%)   | 4 (25)            |
| LV ejection fraction—no. (%)                                  | 31 ± 9            |
| Hypertension—no. (%)  | 14 (87.5)         |
| Diabetes—no. (%)  | 6 (37.5)          |
| Renal failure <sup>b</sup> —no. (%)                           | 7 (43.8)          |
| Estimated glomerular filtration rate (GFR) <sup>c</sup>       | 62.4 ± 24.8       |
| Antiarrhythmic drug—no. (%)                                   | 14 (87.5)         |
| Amiodarone—no. (%)  | 14 (87.5)         |
| The previous type of ICD device                               |                   |
| Indication and type of ICD before the index procedure—no. (%) | 14 (87.5)         |
| Primary prevention—no. (%)                                    | 8 (57.1)          |
| Secondary prevention—no. (%)                                  | 6 (42.9)          |
| ICD implanted after index procedure—no. (%)                   | 2 (12.5)          |
| Previous VT ablation—no. (%)                                  | 4 (25)            |
| Indication for ablation                                       |                   |
| Sustained VT requiring external cardioversion—no. (%)         | 5 (31.3)          |
| Appropriate ICD shock—no. (%)                                 | 11 (68.8)         |
| VT storm—no. (%)  | 7 (43.8)          |

Abbreviations: ICD, implantable cardioverter-defibrillator; LV, Left ventricle; NYHA, New York Heart Association; VT, ventricular tachycardia.

<sup>a</sup>Plus-minus values are means ± SD.

<sup>b</sup>Estimated GFR ≤60 ml/m<sup>2</sup>.

<sup>c</sup>The estimated GFR was calculated with the use of the Cockcroft–Gault formula.

(94%) were male with a mean age of 65 ± 12 years. The structural cause of the VT was ischemic cardiomyopathy (ICM) in 14 (88%), and idiopathic dilated nonischemic cardiomyopathy (NICM) in the remaining 2. The mean LV ejection fraction was 31 ± 9%.

The LV regions most frequently affected by scarring, presenting bipolar voltage <1.5 mV, were located at the septum, inferior, and inferolateral walls (Figure S4). Most patients presented extensive LV scarring, with the mean number of affected segments per patient being 8.0 ± 2.8 (minimum: 3; maximum: 12). Epicardial mapping was performed in three patients (19%), one with ICM and two with NICM. A detailed map during VT was available in 8/16 patients. High-resolution substrate maps collected under different wavefront sources were available for 11 patients.

### 3.2 | Automatic LAVA annotation algorithm assessment

#### 3.2.1 | Gold-standard substrate map

Twenty-nine detailed manual gold-standard substrate maps were obtained: 9 in SR, 13 in RV pacing, and 7 in LV pacing (Table S2). The total chamber surface area was 179.4 cm<sup>2</sup> (IQR: 138.6–214.4) and a scar (defined as a region with bipolar voltage below 1.5 mV at endocardium or below 1.0 mV at epicardium) was present in 99.2 cm<sup>2</sup> (IQR: 70.5–112.8), representing 53.6 ± 13.4% of the total surface. Maps comprised a total of 77 259 EGMs (2664 ± 1253 points per map). The median point density at scar regions was 29 points/cm<sup>2</sup> (IQR: 14–48) and in normal areas was 4 points/cm<sup>2</sup> (IQR: 2–5). Overall, 87.3% of the EGMs were classified as abnormal EGMs, including 65.3% of isolated low-voltage EGMs and 21.1% of LAVAs. The remaining 0.9% of EGMs had a localized bipolar voltage below 0.02 mV and were classified as an inert scar.

#### 3.2.2 | Automatic annotation accuracy at the EGM and map levels

Table 2 presents the accuracy obtained with each algorithm setting, using the manual “gold-standard” classification as a reference. Overall, there was an agreement of manual and automatic “sensitive/standard” LPM annotation in 94.5% of EGMs. In addition, in the subset of LAVA signals, “sensitive/standard” LPM properly annotated 81.1% of the EGMs, which compares to the 23.9% using the wavefront algorithm.

The “gold-standard” substrate maps presented LAVAs in a median surface area of 10.1 cm<sup>2</sup> (IQR: 6.9–16.5), representing 13.3% of the scar area and 7.4% of the total chamber surface area. At the map level, there was a spatial concordance of 88.1% (IQR: 79.0%–93.2%) between the “sensitive/standard” LPM and the manual annotation regarding the anatomical regions with definite LAVAs. This compares to 25.4% (IQR: 15.0%–33.1%) using the wavefront algorithm. Figure 2 and Figure S5 present illustrative LAT substrate maps annotated with the “sensitive/standard” mode, the corresponding “gold-standard” map, and the

**TABLE 2** Accuracy of the automatic annotation of ventricular electrograms using the new late potential map algorithm (in its various sensitivity set modes) and the previous wavefront algorithm

|                       | Number of EGMs | Late potential map algorithm                               |   |   | Wavefront algorithm (correctly annotated/unrecognized/artifact) |
|-----------------------|----------------|--|---|---|---|
|                       |                | Sensitive mode (correctly annotated/unrecognized/artifact) | Sensitive/standard mode (correctly annotated/unrecognized/artifact) | Standard mode (correctly annotated/unrecognized/artifact) |   |
| Overall accuracy      | 77 259         | 92.3%/3.6%/4.1%  | 94.5%/4.0%/1.5%   | 89.8%/9.6%/0.6%   | 83.7%/16.1%/0.2%  |
| Abnormal EGMs         | 68 939         | 93.4%/4.1%/2.6%  | 94.1%/4.6%/1.3%   | 88.6%/11.0%/0.4%  | 81.4%/18.4%/0.2%  |
| LAVAs                 | 16 316         | 83.1%/16.7%/0.2%   | 81.1%/18.7%/0.2%  | 54.7%/45.2%/0.1%  | 23.9%/76.1%/0%  |
| Definite LAVAs        | 9319           | 83.0%/16.9%/0.1%   | 84.6%/15.3%/0.1%  | 49.8%/50.1%/0.1%  | 17.1%/82.9%/0%  |
| Intra-far-field LAVAs | 6997           | 83.2%/16.7%/0.1%   | 76.4%/23.5%/0.1%  | 61.2%/38.7%/0%  | 32.8%/67.2%/0%  |

Note: Sensitive/standard mode means sensitive in the areas with bipolar voltage <1.0 mV and standard mode in the remaining regions.

Abbreviations: EGM, electrogram; LAVA, local abnormal ventricular activity.

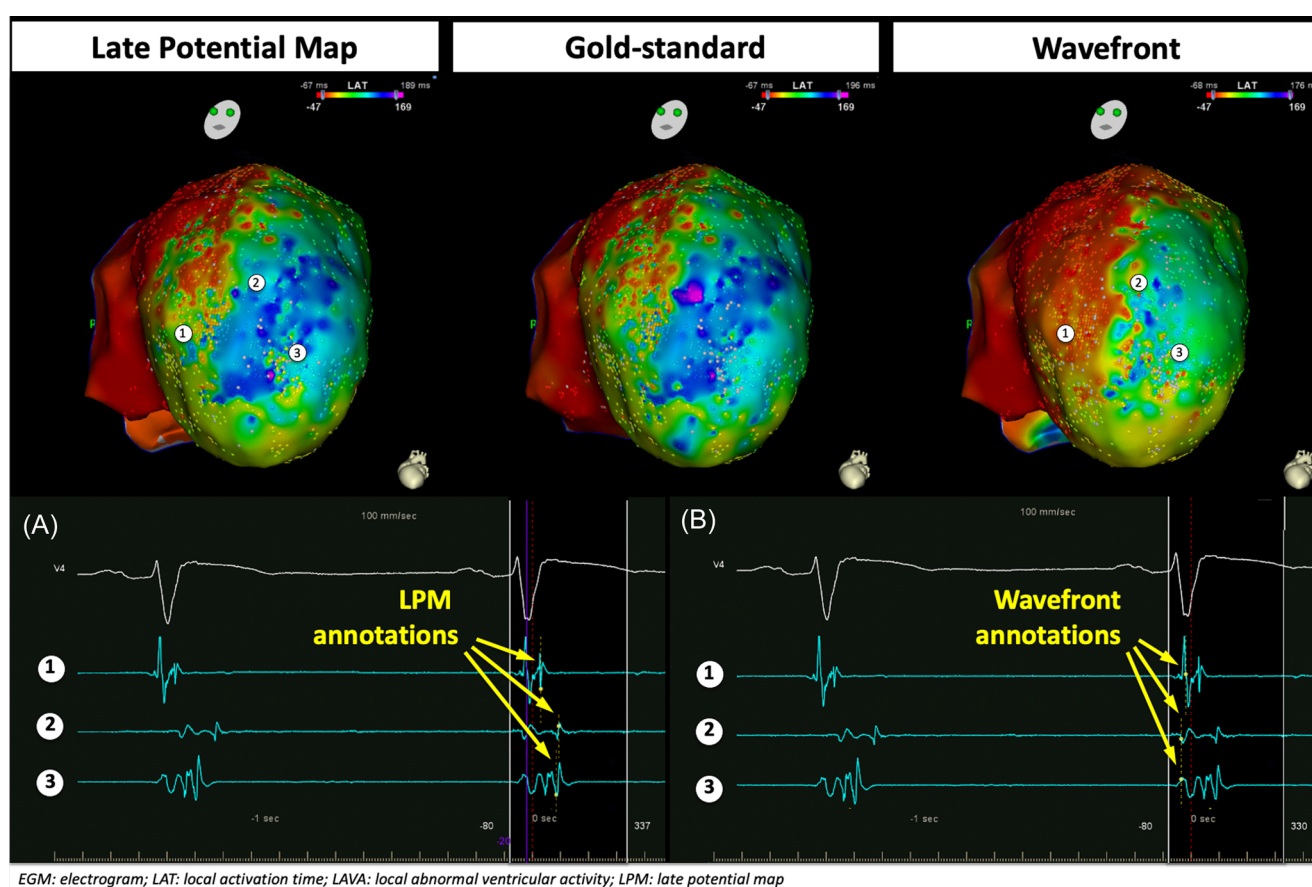
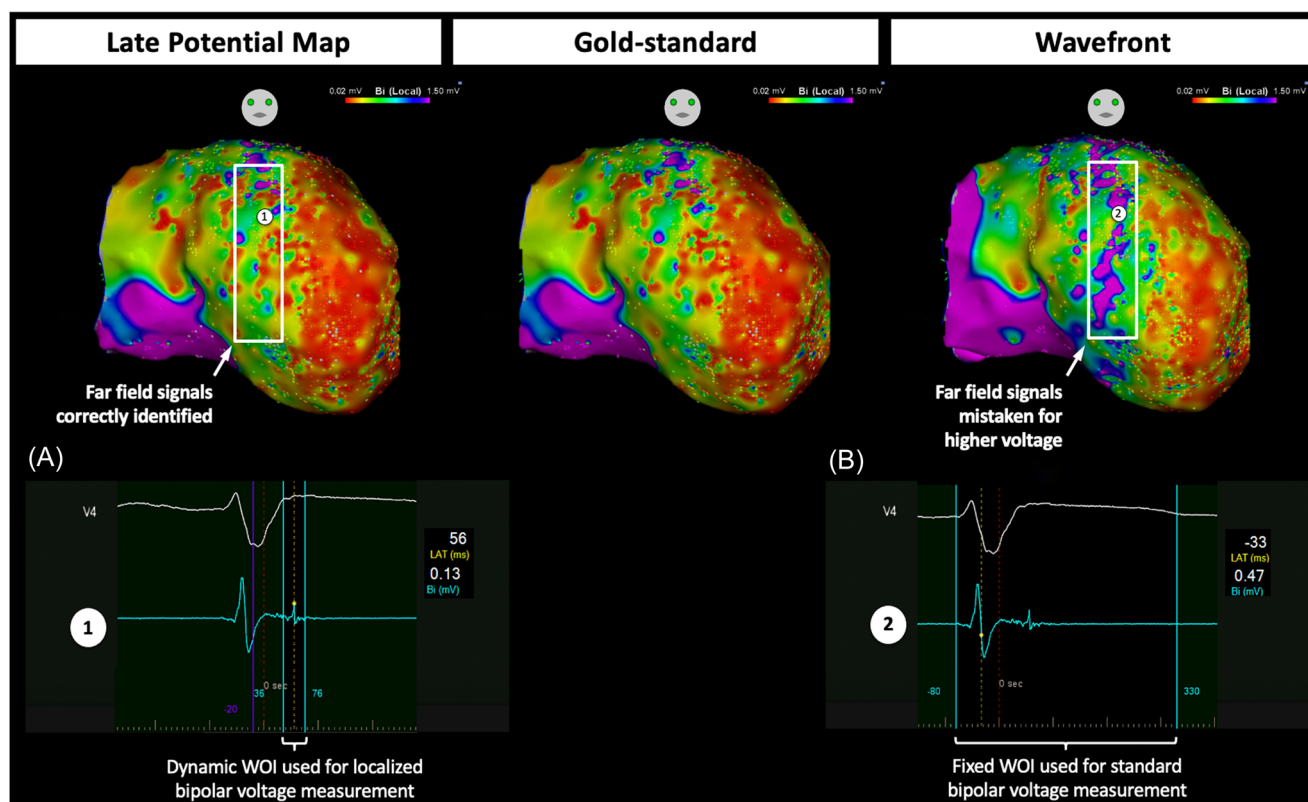


**FIGURE 2** Comparison of the LAT substrate map automatically annotated (LPM sensitive/standard mode) in an ICM patient with the “gold-standard” manually annotated map. The LPM algorithm properly annotated 92.8% of signals (2515/2711), including 84.1% of definite LAVAs (371/441) and 73.2% of intra-far-field LAVAs (259/354). The spatial concordance of the maps was 96.5%. The wavefront algorithm failed in annotating the near-field component in 80.5% of LAVAs, resulting in high spatial discordance. (A, B) Present illustrative EGMs are properly annotated by the LPM and misannotated by the wavefront algorithm, respectively. EGM, electrogram; ICM, ischemic cardiomyopathy; LAT, local activation time; LAVA, local abnormal ventricular activity; LPM, late potential map

map annotated with the wavefront algorithm. Figure S6 depicts the spatial concordance of all the 29 maps.

The performance of the algorithm at the epicardium was comparable to the one observed at the endocardium, with no

differences in the “sensitive/standard” LPM accuracy regarding the annotation of LAVAs both at the EGM level (epicardium: 82.8% vs. endocardium: 80.9%,  $p = \text{NS}$ ) and map level (epicardium: 88.3% vs. endocardium: 84.9%,  $p = \text{NS}$ ).



EGM: electrogram; LAT: Local Activation Time; LPM: late potential map; WOI: Window of Interest

**FIGURE 3** Comparison of the localized bipolar substrate map automatically annotated with the LPM software (sensitive/standard mode) with the “gold-standard” and wavefront algorithm maps. On top of providing a proper LAT annotation, LPM software applied a dynamic WOI, excluding the far-field component from the voltage amplitude measurement. Note the strand of apparent higher voltage amplitude that could be mistakenly taken as a channel of viable tissue, but actually represents far-field signal voltage (white box). (A, B) Present an illustrative EGM from that strand and its bipolar voltage measurement using the LPM software and the wavefront algorithm, respectively. EGM, electrogram; LAT, local activation time; LPM, late potential map; WOI, window of interest

### 3.2.3 | EGM characterization in terms of localized bipolar voltage

Figure 3 represents the map level repercussion of localized bipolar voltage measurement, based on the use of a dynamic WOI that excludes the far-field component from the voltage amplitude measurement in complex EGMs, in comparison with the standard evaluation, which applies a fixed WOI. Often, in the latter, apparent regions of higher voltage that could be mistakenly taken as channels of viable tissue actually represented far-field signal voltage.

Table 3 presents the localized bipolar voltage of the EGM. Among abnormal EGMs, the localized bipolar voltage significantly differed with respect to the EGM type ( $p < .001$ ). In particular, the LAVAs' localized bipolar voltage was significantly higher than isolated low-voltage EGMs (0.22 [IQR: 0.10–0.44] versus 0.13 mV [IQR: 0.05–0.40],  $p < .001$ ). Among LAVAs, it was significantly lower for definite than intra-far-field LAVAs ( $p < .001$ ). Figure S7 depicts the distribution of the 16 316 LAVA signals regarding the localized bipolar voltage. The heterogeneous distribution of localized bipolar voltage within categories and the overlap between categories resulted in its incapacity to distinguish LAVAs from the remaining

abnormal EGMs. The receiver operator characteristic curve analysis showed a modest accuracy of localized bipolar voltage in distinguishing LAVAs from other abnormal EGMs (area under the curve: 0.676; 95% confidence interval: 0.672–0.680;  $p < .001$ ) (Figure S8).

## 3.3 | LCV analysis

### 3.3.1 | VT circuit topography

Eight detailed VT activation maps providing appropriate delineation of the critical isthmus were analyzed (2151 ± 1242 points per map). The mean QRS duration was 199 ± 28 ms and the tachycardia cycle length of 479 ± 70 ms (range: 378–597 ms). Activation maps demonstrated reentrant circuits with a variety of isthmus morphologies, with a median VT isthmus length, width, and area of 33 mm (IQR: 30–48), 11 mm (IQR: 9–15), and 7.2 cm<sup>2</sup> (IQR: 4.7–8.5), respectively. The macroreentrant circuit comprised a single outer loop in two patients and a dual-loop mechanism in six. All VT maps presented at least one portion of the VT isthmus with LCV ≤ 0.20 mm/ms. Within the VT isthmus, the slowest region varied: in four patients (50%), it

**TABLE 3** Localized bipolar voltage by electrogram category

| EGM category |                          |                      | Number of EGMs (total: 77 259) | Median (IQR), mV |
|--------------|--------------------------|----------------------|--------------------------------|------------------|
| Normal EGM   |                          |                      | 9789                           | 2.82 (2.00–4.42) |
| Abnormal EGM | Isolated low-voltage EGM |                      | 50 435                         | 0.13 (0.05–0.40) |
|              | LAVA                     | Definite LAVA        | 9319                           | 0.15 (0.08–0.30) |
|              |                          | Intra-far-field LAVA | 6997                           | 0.34 (0.18–0.63) |
|              | Inert scar               |                      | 719                            | 0.02 (0.01–0.02) |

Abbreviations: EGM, electrogram; IQR, interquartile range; LAVA, local abnormal ventricular activation; mV, millivolts.

was the entrance region; in one, it was the exit region; in one, it was the isthmus common channel; and the remaining two patients presented LCV equally slow at the entrance/common channel or common channel/exit, respectively (Table S3).

### 3.3.2 | Relationship between VT activation map and substrate map

The localized bipolar voltage amplitude at VT isthmus sites during sinus or paced rhythm was consistently  $\leq 0.5$  mV in all cases. LCV analysis in high-density substrate maps identified a median of two intrascar conduction corridors per patient (IQR: 2–3), including the one acting as VT isthmus in all cases ( $n = 8$ , 100%) (Figures 4–6). Most of the patients had channels with multiple entries ( $n = 7$ ; 87.5%) and some had interconnected channels ( $n = 3$ ; 37.5%). Finally, slow conduction patches, not forming channels, with velocity vectors in a side-by-side distribution, were seen at the outer border zone of the scar in seven patients (87.5%).

The median intrascar conduction corridors area was significantly lower than the overall LAVAs area (4.4 [IQR: 3.15–7.3] versus 10.6 cm<sup>2</sup> [IQR: 6.0–17.5],  $p = .012$ ), but it was not significantly different from the VT isthmus area (4.4 [IQR: 3.15–7.3] versus 7.2 cm<sup>2</sup> [IQR: 4.7–8.5],  $p = .123$ ).

## 3.4 | Clinical outcomes

The ablation strategy was not modified because of participation in this study. Vascular access complications occurred in one patient, without further acute adverse events. During a median follow-up of 17 months, two patients had VT recurrence and three patients died

due to end-stage heart failure related-events. The estimated VT ablation success rate at 2 years was 83% (Figure S9).

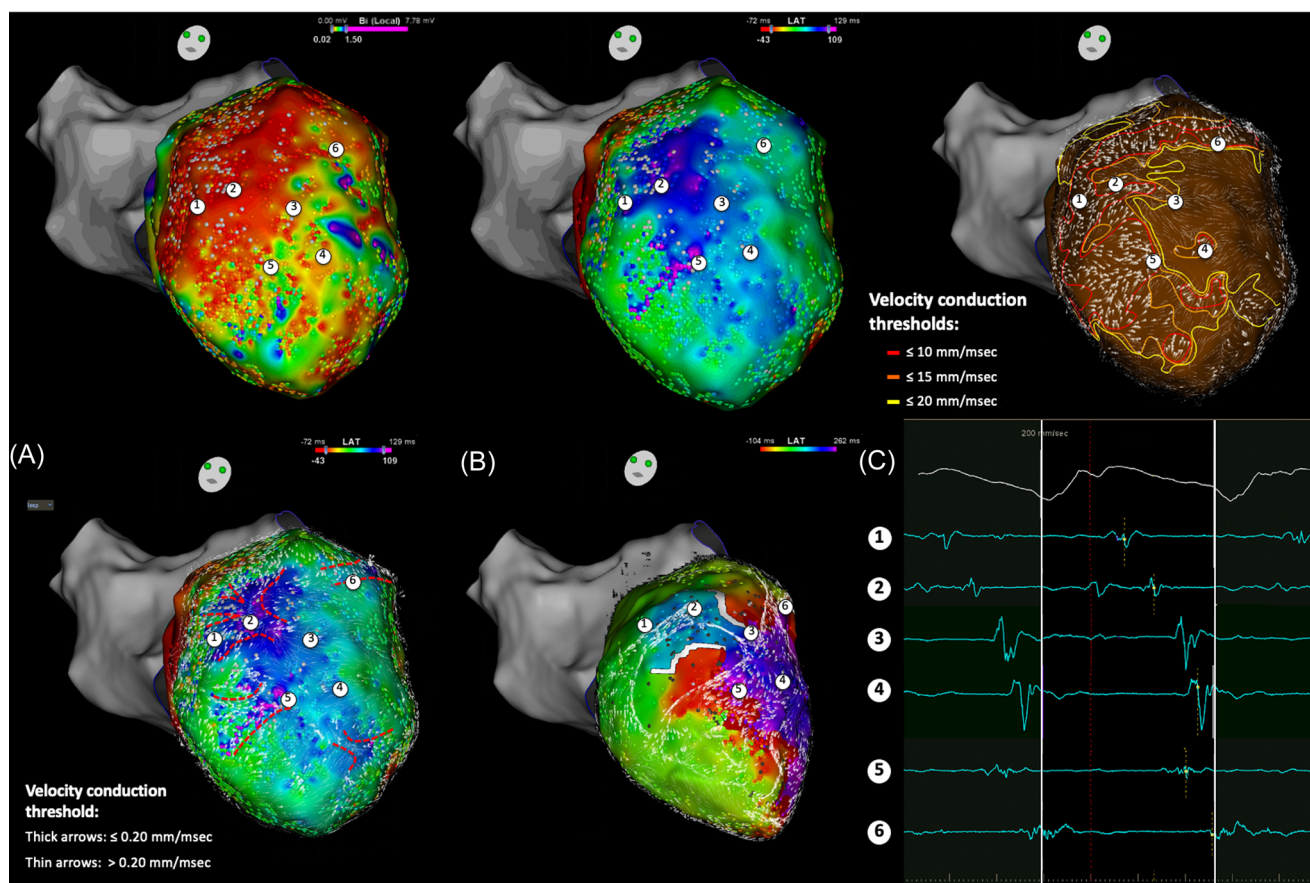
## 4 | DISCUSSION

The major findings of this study were:

1. At the EMG level, the new LPM algorithm using the “sensitive/standard” mode had an overall accuracy of 94.5% and a LAVA identification accuracy of 81.1% compared to a gold-standard manual assessment—this contrasts with an 83.7% and 23.9% accuracy using the wavefront algorithm.
2. At the map level, it allowed a spatial concordance of 88.1% compared to a gold-standard assessment.
3. Localized bipolar voltage had only modest accuracy in distinguishing LAVA from other abnormal EGMs.
4. LCV analysis in high-density substrate mapping allowed the identification of intrascar conduction corridors, including the ones acting as VT isthmuses.

Substrate mapping focuses on the identification of LAVAs. Automated annotation algorithms were developed to optimize and decrease procedural time, allowing for rapid acquisition of high-resolution substrate maps.<sup>1,2</sup> However, these may annotate far-field rather than near-field signals in areas of low voltage, rendering the resulting maps hard to interpret.<sup>3</sup> Furthermore, the latency and the ability to detect LAVAs are dependent on the activation wavefronts with a variable fusion of the EGM components and thus are affected to a large extent by the anatomical locations of scar.<sup>5</sup> The previous wavefront algorithm<sup>6</sup> uses both bipolar and unipolar signals from a pair of electrodes for LAT annotation. The new LAA relies on the





All EGMs are displayed at a similar gain of 0.20 mm/mV. LCV maps were calculated applying a velocity threshold of 0.20 mm/msec. Compression levels of 2 and 3 were used in the sinus rhythm and VT activation map, respectively. EGM: electrogram; ICM: ischemic cardiomyopathy; LPM: local potential map; LAT: local activation time; LCV: local conduction velocity; VT: ventricular tachycardia.

**FIGURE 4** Substrate maps automatically annotated with the LPM algorithm, displayed as localized bipolar voltage map, LAT map, and LCV map in an ICM patient. The arrows in the LCV map represent the local vectors and are displayed as thick in the sites where conduction is slower than a certain threshold. In this example, the zones with LCV below 0.20, 0.15, and 0.10 were delineated with red, orange, and yellow lines, and were distributed throughout the scar and at the border zone. (A) LCV vectors were superimposed on the LAT substrate map and vector compression was applied to identify the dominant slow conduction vectors. In this patient, four intrascar conduction corridors were recognized, composed of low LCV vectors ( $\leq 0.20$  mm/ms) with orientation parallel to the length of the corridor and length  $\geq 10$  mm, extending into the areas with late potentials, and appear highlighted with dashed red lines. (B) VT activation map, revealing a figure-of-eight macroreentrant circuit. In the maps, Numbers 1–6 were positioned at the same anatomical locations, and their corresponding EGMs during VT are presented in (C). The comparison of the substrate maps with the VT activation map suggests that the slow conduction zones participate as critical sites for the macroreentrant circuit, acting as entrance region (1, LCV: 0.11 to 0.15 mm/ms) or exit region (3 and 4, LCV ranging from 0.11 to 0.20 mm/ms). The common isthmus corresponded to a site displaying late potentials and moderately reduced LCV (0.16–0.20 mm/ms). The lateral boundaries of the VT channel corresponded to zones with functional blocks, displaying LCV below 0.20 mm/ms during sinus rhythm. All EGMs are displayed at a similar gain of 0.20 mm/mV. LCV maps were calculated by applying a velocity threshold of 0.20 mm/ms. Compression levels of 2 and 3 were used in the sinus rhythm and VT activation map, respectively. EGM, electrogram; ICM, ischemic cardiomyopathy; LPM, late potential map; LAT, local activation time; LCV, local conduction velocity; LPM, late potential map; VT, ventricular tachycardia

same principles of unipolar and bipolar signal analysis but incorporates in the annotation decision process information on the timing, giving priority to the latest component, and the signal consistency in consecutive beats, which increases the annotation accuracy for extremely low-voltage amplitude signals. Indeed, the LAVA identification accuracy was 81.1%, as compared to 23.9% using the previous wavefront algorithm. In addition, this new algorithm is flexible. If LAVAs are not being properly recognized in a certain anatomical region, for instance, because they are occurring early in the QRS or even preceding the ventricular far-field component, it is possible to improve the annotation accuracy by using specific tools for regional

modification of EGM annotations. These tools allow a) readjustment of the late boundary threshold to an earlier time value; b) readjustment of the LPM sensitivity mode, making the algorithm more sensitive or more specific; and c) readjustment of the WOI, which allows to reannotate the uncommon LAVAs that precede far-field signals.

Substrate mapping also depends on factors affecting the size and shape of EGMs, namely mapping electrode size and interelectrode spacing. Mapping catheters with small electrodes and small interelectrode distance have identified sharp and high-voltage signals in areas previously considered to be a dense scars, in



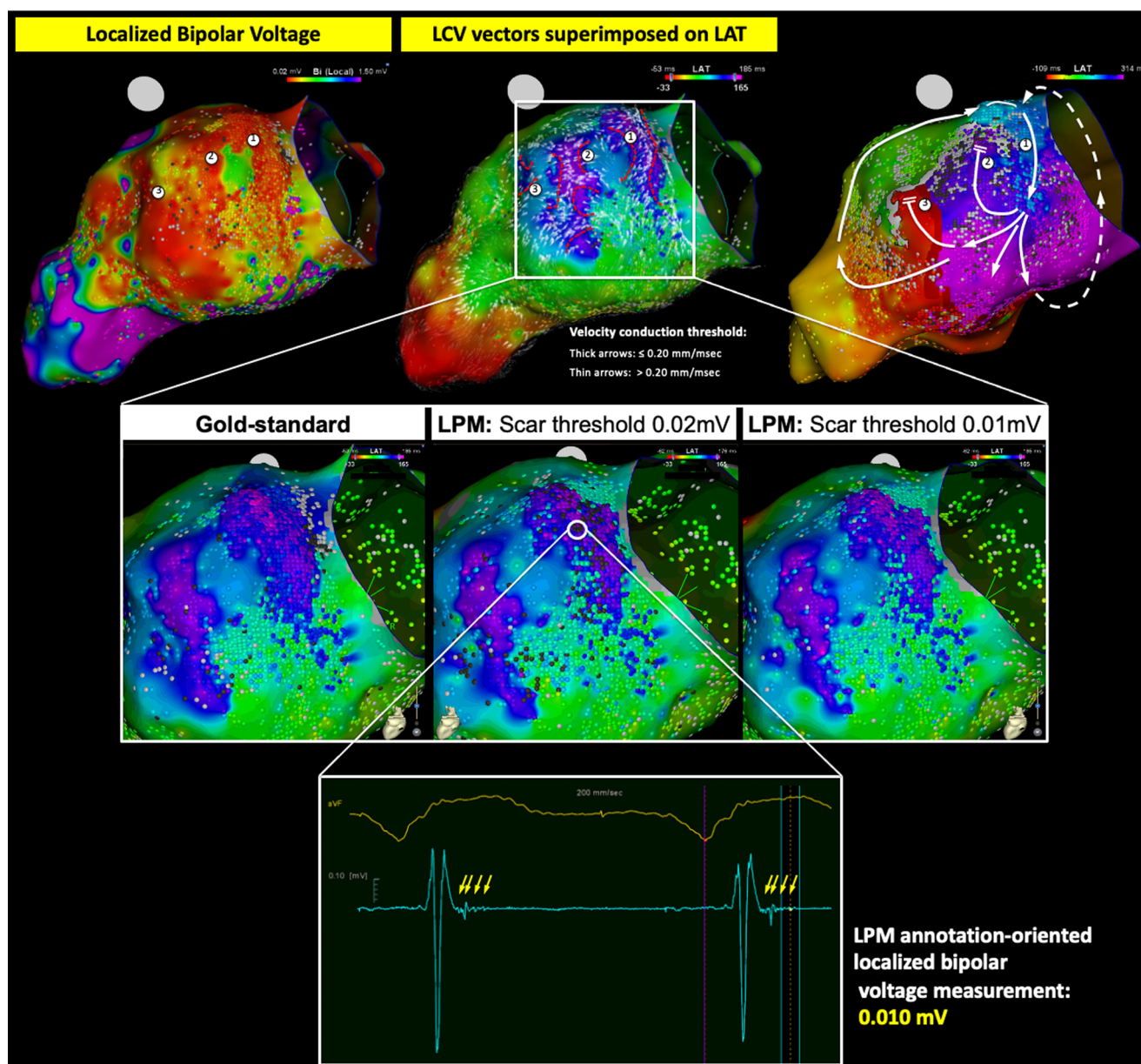


**FIGURE 5** Comparison of the substrate maps collected during RV pacing and annotated with the LPM algorithm with the corresponding VT activation map in an ICM patient. The LCV vectors superimposed on the LAT substrate map suggest the presence of three intrascar conduction corridors (1–3), highlighted with a red dashed lines. Comparing the substrate maps with the VT activation map suggests that isthmus (1) and dead ends (2, 3) co-locate with the intrascar conduction corridors, occurring functional block during VT in both dead ends. At the area of interest, shown in the middle panel, the “gold-standard” map was very similar to the automatic LPM map using the scar threshold of 0.02 mV and was almost indistinguishable from the one with scar threshold reduction to 0.01 mV. Indeed, various EGMs within the critical intrascar conduction corridor presented extremely low-voltage near-field components (0.01 mV) properly annotated by the algorithm (bottom panel). All EGMs are displayed at a similar gain of 0.20 mm/mV. LCV vectors were calculated by applying a velocity threshold of 0.20 mm/ms and a compression level of 2. EGM, electrogram; ICM, ischemic cardiomyopathy; LAT, local activation time; LCV, local conduction velocity; LPM, late potential map; RV, right ventricle; VT, ventricular tachycardia

relation to surviving myocardial bundles.<sup>2,7,8</sup> In this study, combining the Pentaray<sup>®</sup> catheter with 2 mm electrode spacing with an algorithm for localized bipolar voltage measurement, we showed that the median specific voltage of LAVA was 0.22 mV (IQR: 0.10–0.44). Although significantly different, localized bipolar

voltage has only modest accuracy in distinguishing LAVAs from other abnormal EGM.

Until now, the quantitative assessment of LCV remained an unmet need in the electroanatomical mapping systems. Therefore, LCV has been evaluated indirectly through visual analysis of isochronal LAT



## REFERENCES

1. Launer H, Clark T, Dewland T, Henrikson CA, Nazer B. An automated fractionation mapping algorithm for mapping of scar-based ventricular tachycardia. *Pacing Clin Electrophysiol*. 2019;42:1133-1140.
2. Viswanathan K, Mantziari L, Butcher C, et al. Evaluation of a novel high-resolution mapping system for catheter ablation of ventricular arrhythmias. *Heart Rhythm*. 2017;14:176-183.
3. Knecht S, Spies F, Altmann D, Reichlin T, Sticherling C, Kühne M. Electroanatomic mapping of atrial tachycardia—manual vs automated annotation. *Heart Rhythm Case Rep*. 2017;3:145-147.
4. Anter E, Kleber AG, Rottmann M, et al. Infarct-related ventricular tachycardia: redefining the electrophysiological substrate of the isthmus during sinus rhythm. *JACC Clin Electrophysiol*. 2018;4:1033-1048.
5. Komatsu Y, Daly M, Sacher F, et al. Electrophysiologic characterization of local abnormal ventricular activities in postinfarction ventricular tachycardia with respect to their anatomic location. *Heart Rhythm*. 2013;10:1630-1637.
6. El Haddad M, Houben R, Stroobandt R, Van Heuverswyn F, Tavernier R, Duytschaever M. Novel algorithmic methods in mapping of atrial and ventricular tachycardia. *Circ Arrhythm Electrophysiol*. 2014;7:463-472.
7. Tschabrunn CM, Roujol S, Dorman NC, Nezafat R, Josephson ME, Anter E. High-resolution mapping of ventricular scar: comparison between single and multielectrode catheters. *Circ Arrhythm Electrophysiol*. 2016;9(6):e003841.
8. Anter E, Tschabrunn CM, Buxton AE, Josephson ME. High-resolution mapping of postinfarction reentrant ventricular tachycardia: electrophysiological characterization of the circuit. *Circulation*. 2016;134:314-327.
9. Aziz Z, Shatz D, Raiman M, et al. Targeted ablation of ventricular tachycardia guided by wavefront discontinuities during sinus rhythm. *Circulation*. 2019;140:1383-1397.
10. Anter E, Neuzil P, Reddy VY, et al. Ablation of reentry-vulnerable zones determined by left ventricular activation from multiple directions: a novel approach for ventricular tachycardia ablation: a multicenter study (PHYSIO-VT). *Circ Arrhythm Electrophysiol*. 2020;13:539-550.

## SUPPORTING INFORMATION

Additional supporting information can be found online in the Supporting Information section at the end of this article.

**How to cite this article:** Cortez-Dias N, Lima da Silva G, Nunes-Ferreira A, et al. Novel "late potential map" algorithm: abnormal potentials and scar channels detection for ventricular tachycardia ablation. *J Cardiovasc Electrophysiol*. 2022;33:1211-1222. doi:10.1111/jce.15470